

Article

Functional Control Engineering of Coal Gangue Electrocatalyst with Amorphous SiC_x/SiO_x Active Layer Loading Enables Efficient Li-O₂ Batteries

Zhihui Sun , Nan Zhou *, Meng Li, Jianfei Xu, Wenchang Feng and Shuo Liu

School of Mines, China University of Mining and Technology, Xuzhou 221116, China

* Correspondence: 5724@cumt.edu.cn

Abstract: The unreasonable accumulation of coal gangue in mining areas has caused serious resource waste and environmental pollution. The functional utilization of coal gangue with high added value has become the key to solving the previous problem. Coal gangue has inherent advantages such as large specific surface areas and rich active components, giving rise to an excellent precursor of electrode material in electrochemical energy storage devices. Herein, we, firstly, fabricated an amorphous SiC_x/SiO_x electrocatalyst with an abundant oxygen vacancy by acid–alkali activation derived from coal gangue for advanced Li-O₂ batteries. The in-depth experimental results coupled with an in situ characterization analysis revealed that the amorphous SiC_x/SiO_x layer with abundant functional groups and oxygen vacancies on the surface of the activated gangue was conducive to promote structural stability and to improve the formation/decomposition efficiency of discharged products (Li₂O₂). Therefore, the LOBs based on the activated coal gangue electrocatalyst delivered a low overpotential of 1.12 V, high discharge capacity of 9156 mAh g⁻¹, and an improved cyclic stability (more than 350 h). This work can provide a new approach for the development of new functions of coal gangue.

Keywords: coal gangue; surface modification; high value-added utilization; bifunctional electrocatalysts; Li-O₂ battery



Citation: Sun, Z.; Zhou, N.; Li, M.; Xu, J.; Feng, W.; Liu, S. Functional Control Engineering of Coal Gangue Electrocatalyst with Amorphous SiC_x/SiO_x Active Layer Loading Enables Efficient Li-O₂ Batteries. *Appl. Sci.* **2023**, *13*, 5551. <https://doi.org/10.3390/app13095551>

Academic Editor: Andrea L. Rizzo

Received: 29 March 2023

Revised: 24 April 2023

Accepted: 26 April 2023

Published: 29 April 2023



Copyright: © 2023 by the authors. Licensee MDPI, Basel, Switzerland. This article is an open access article distributed under the terms and conditions of the Creative Commons Attribution (CC BY) license (<https://creativecommons.org/licenses/by/4.0/>).

1. Introduction

Aprotic lithium–oxygen batteries (LOBs) have emerged as a promising alternative candidate for large-scale energy storage and practical electric vehicle applications by virtue of their low cost, non-pollution, and high theoretical energy density (3500 Wh kg⁻¹) [1,2]. In 1996, the concept of secondary LOBs was first proposed, which set off a wave of research in the field [3]. However, to achieve large-scale commercial applications of LOBs, there are still many key scientific issues that need to be resolved, including the low activity of the positive electrode catalyst, serious polarization, and poor cycle stability [4,5]. These problems can be attributed to the slow kinetics of oxygen reduction (ORR) and oxygen evolution (OER) reactions in LOBs during cycling [6,7]. The introduction of high-efficiency and stable electrocatalysts can significantly increase the rate of oxygen reduction and oxygen evolution reactions, thereby reducing the overpotential during cycling and improving the overall performance of LOBs [8,9]. The general working mechanism of typical LOBs could be summarized as follows: O₂ (diffusion from the cathode) can react with Li⁺ (coming from the anode) to form a discharge product (Li₂O₂) on the surface of the cathode in the discharge process, which could be, subsequently, decomposed after the following charging [10]. Therefore, the preparation of cathode materials with high catalytic activities and structural stabilities is the key to the development of LOBs [11]. Thus far, many catalytic materials have been widely fabricated and applied in LOBs, such as carbonaceous materials, noble-metal-based electrocatalysts, transitional metal oxide, etc. [12]. In order

to achieve an efficient balance between the cost and electrochemical activity of cathode materials, the utilization of coal-based solid waste has become quite a good choice.

Coal gangue is the main associated waste in the process of coal mine construction, mining, and washing [13]. It is a hard mixture with a low carbon content and complex composition (mainly containing SiO_2 and Al_2O_3) [14]. Coal gangue has a loose and porous needle-like flake structure with apparent densities ranging from 1960 kg/m^3 to 2760 kg/m^3 [15]. On the one hand, the clay minerals kaolinite and bentonite, which are rich in coal gangue, have unique lamellar structures and surface chemical properties. The unique lamellar structures could provide sufficient storage space for discharge products and surface chemical properties with excellent adsorption performance, which could improve the formation/decomposition efficiency of discharge products, giving rise to a well-knit Li_2O_2 formation [16]. On the other hand, there are abundant adsorption sites and abundant hydroxyl groups on the surfaces of coal gangue, which are prone to interfacial reactions [17]. The enhanced adsorption sites and hydroxyl groups could act as the active sites for oxygen reduction and oxygen evolution reactions to further improve the electrochemical performances of LOBs [18]. Thus, coal gangue is an ideal precursor for constructing highly active electrochemical materials in energy storage devices (especially LOBs). However, the complex composition of coal gangue has been proven to be the main reason hindering its efficient comprehensive utilization. Coal gangue contains a variety of trace heavy metal elements, such as lead, zinc, cadmium, arsenic, chromium, etc., which are non-degradable, carcinogenic, teratogenic, and bring potential environmental risks [19,20]. In addition, the organics and minerals in coal gangue are easily oxidized in lithium–air batteries to form various harmful substances, such as nitrogen oxides and sulfides [21]. The functional modification and high-value utilization of coal gangue has become an important research topic to solve the overall planning of mineral development and environmental protection.

The functional modification of coal gangue refers to the mineral materials with electrical, optical, thermal, and other functional effects prepared by coal gangue after deep processing or fine processing [22]. Zhang et al. fabricated the metal-free composite of coal gangue and graphite carbon nitride ($\text{g-C}_3\text{N}_4$) as the degradation catalytic material [23]. Coal gangue with rich hydroxyl groups can induce the formation of double-nitrogen defects (cyanogroup and nitrogen vacancies) for $\text{g-C}_3\text{N}_4$, thus reducing the C-N band gap and adsorption energy for peroxydisulfate (PMS). The composite can oxidize PMS to achieve efficient degradation of bisphenol A (BPA) without the assistance of light, electricity, or other energy sources. Mei et al. modified the gangue mineral by a simple phase transformation reaction, and the activated mineral obtained had lower crystallinity and higher surface disorder, thus showing excellent catalytic activity for hydrogen evolution (HER) and the oxygen evolution reaction (OER) [24]. Dong et al. anchored CuFe_2O_4 nanoparticles on kaolinite with Fe-O-Al chemical bonding by the calcination method. The hydroxyl groups present on the surface of the kaolinite could effectively solve the problem of nanoparticle agglomeration and increase the reactive sites [25]. The CuFe_2O_4 /kaolinite exhibited high photocatalytic activity for BPA and low leaching of metal ions. Sun et al. synthesized a layered C/SiO_x composite with a porous skeleton structure derived from coal gangue, which showed high electrochemical performance in Li-ion batteries. These studies indicated that there are a lot of adsorption sites and abundant hydroxyl groups on the surface of coal gangue, which make coal gangue an ideal precursor for constructing highly active electrochemical materials [26]. However, natural coal gangue is rarely used in the field of electrochemical energy storage due to its complex mineral composition and low electrochemical activity [27]. Therefore, the controllable design of coal-gangue-based hybrid electrocatalysts still needs further development to break the bottleneck.

Herein, a coal gangue with an amorphous structure was, firstly, fabricated and applied as a bifunctional cathode electrocatalyst for LOBs. An amorphous protective layer was in situ fabricated on the surface of coal gangue by the well-designed acid–base activation treatment, while abundant highly active functional groups and oxygen vacancies were in-

produced. The activated coal gangue demonstrated a superior electrochemical performance and a long cyclic life. According to in-depth analysis, the synergistic interaction between SiC_x and SiO_x , the distinctive amorphous structures, and the substantial active sites were critical factors in contributing to good electrochemical performance. Impressively, this is the first time that mined solid waste with modified treatment was proven to be a brilliant cathode electrocatalyst for LOBs.

2. Materials and Methods

2.1. Synthesis of Activated Coal Gangue Precursor

In total, 2.5 g of crushed coal gangue powder was dissolved in 100 mL ammonia water, and then the mixture was placed in an ultrasonic cleaner for 2 h. Next, the precipitates were centrifuged with deionized water and ethanol 3~4 times to remove the side products and dried at 60 °C, respectively. The dry powder was mixed with sodium carbonate (Na_2CO_3) with a mass ratio of 10:6. The mixture was treated by high-energy ball milling for at least 4 h and then was calcined at 875 °C for 2.5 h.

2.2. Synthesis of Activated Coal Gangue

The precursor was vigorously stirred in dilute sulfuric acid (H_2SO_4) solution for 1 h, centrifuged with deionized water and ethanol 3~4 times to remove the side products, and dried at 60 °C, respectively. The dry intermediate product was mixed and vigorously stirred with a sulfuric acid solution (6 mol/L), and then the pH of the solution was adjusted to 2 by adding deionized water. Finally, the resulting mixture was centrifuged with deionized water and ethanol 3~4 times to remove impurities, and the final precipitation was collected and dried at 60 °C.

2.3. Materials Characterization

The samples' micro-morphologies and structures were determined by a Hitachi SU8010-Scanning electron microscope (SEM, TESCAN, Brno, Czech Republic) and a D8 Advance X-ray diffractometer (XRD, Bede Scientific Ltd., Durham, UK). The elements' compositions, chemical states, molecular structures, and other aspects of the samples were tested by Escalab 250Xi- X-ray photoelectron spectroscopy (XPS, VG ESCALAB MKII, VG Scientific, Cambridge, UK).

2.4. Electrochemical Measurement

The as-prepared gangue-based electrocatalyst powder was mixed with super P (acted as conductive agent) and Polyvinylidene fluoride (acted as binder) at a weight ratio of 7:2:1 and then dissolved in 1-Methyl-2-pyrrolidinone (NMP) under continuous stirring. The homogeneous slurry was sprayed onto carbon paper with a mass loading of $0.5 \pm 0.2 \text{ mg cm}^{-2}$, and the final whole carbon paper was used as the working electrode. In total, 1 M lithium bis (trifluoromethane sulphonamide, LiTFSI) was dissolved in dimethyl sulfoxide (DMSO), and the solution was applied as electrolyte. The 2032-LOBs contained a lithium metal anode ($\Phi = 16 \text{ mm}$), a glass-fiber separator (GFC, Whatman, $\Phi = 19 \text{ mm}$), and a gangue-based cathode ($\Phi = 13 \text{ mm}$), which must be assembled in the customized glove box filled with pure Ar. The assembled LOBs were measured in a homemade sealed glass bottle filled with high-purity O_2 to evaluate the electrochemical properties. The galvanostatic discharge–charge tests were carried out on a LAND BT 2000 battery testing system. Cyclic voltammetry (CV) and electrochemical impedance spectroscopy (EIS) were tested via an electrochemical workstation (CHI600E, Shanghai Chenhua Instrument Co., Ltd., Shanghai, China). All current densities and specific capacities of the LOBs were normalized by the actual mass loading of the active materials.

3. Results and Discussion

3.1. Analysis for the Fabrication of Activated coal Gangue Precursor

As shown in Figure 1, the activated coal gangue with an amorphous structure was, firstly, prepared by a series of simple alkali–acid activation steps. Specifically, the alkaline environment formed by early ammonia impregnation softened the Si–O species on the surface of the coal gangue, which promoted the formation of the pore structure and reduced the activation energy of the coal gangue. In the following calcination process, sodium carbonate reacted with activated silicon oxide to form a NaAlSiO_4 passivation layer on the surface of the coal gangue (Figure S1). Finally, the NaAlSiO_4 passivation layer was acidified by multiple acid immersion to facilitate the formation of amorphous silicon oxide, and unwanted oxide impurities on the surface of coal gangue were dissolved and removed at the same time. In addition, it should be emphasized that the decomposition efficiencies of the impurities were mainly related to the concentration of H^+ , thus we adjusted the pH value of the last amount of sulfuric acid to 2 to ensure that there were enough hydrogen ions to fully remove the impurities on the surface of the coal gangue.

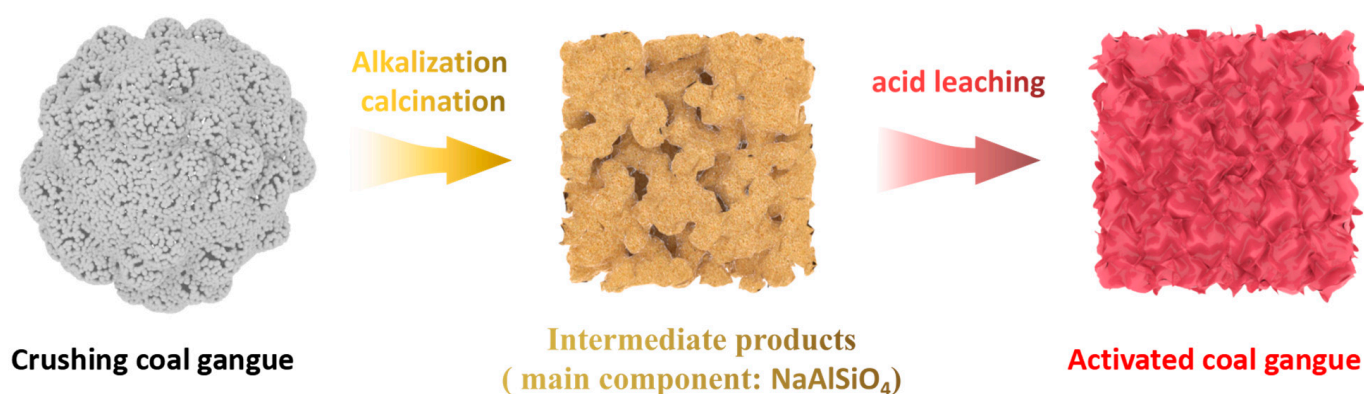


Figure 1. Schematic illustration of the preparation of activated coal gangue.

3.2. Morphological and Structural Characterization

Scanning electron microscope (SEM) analysis was conducted to feature the micro-morphology differences of the coal gangue during the fabrication process. As shown in Figure 2a, the crushed coal gangue after simple ball milling delivered the coexisting structure of the bulk and layered particles, and the particle sizes ranged between 2–10 microns. The high-resolution SEM in Figure 2b further indicated that the surface of the coal gangue particles had rich folds and porous skeleton structures. After the acid and alkali activation, the activated coal gangue showed a loose and porous colloidal structure with a nanometer scale (Figure 2c). Figure 2d demonstrated that the surface of activated coal gangue contained abundant microporous and macroporous structures. The macropores were conducive to the full infiltration of electrolyte and provided sufficient space for the accumulation of discharge products, while the micropores could promote the ion diffusion rate in the electrode reaction during the discharge–charge process in the LOBs [14]. In addition, the unique colloidal nano-morphology could ensure sufficient exposure of the active sites on the surface of the activated coal gangue. In short, the acid and alkali activation reaction effectively optimized the surface morphologies of the coal gangue, leading to the improvement of the electrocatalytic activity in the LOBs.

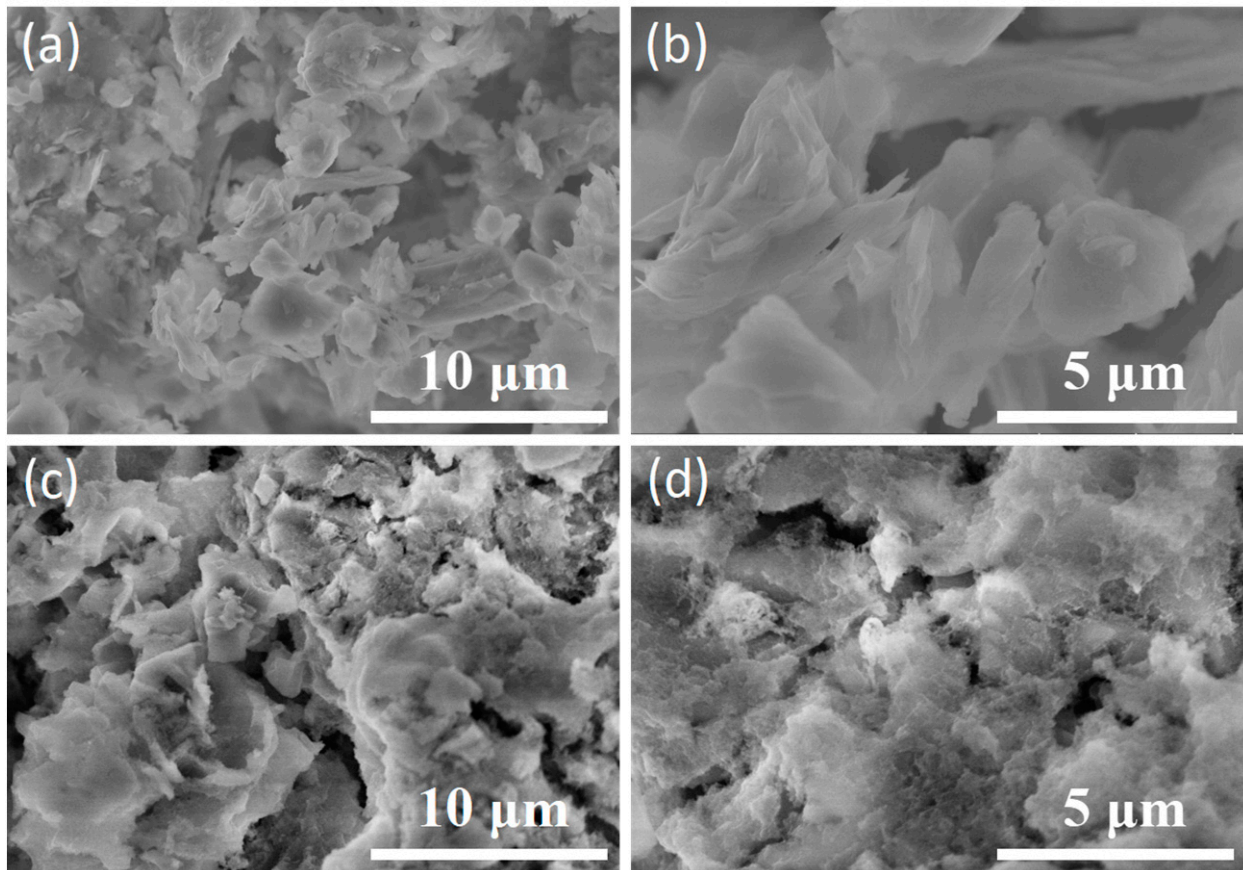


Figure 2. (a) SEM image of crushed coal gangue; (b) High-resolution SEM image of crushed coal gangue; (c) SEM image of activated coal gangue; (d) High-resolution SEM image of activated coal gangue.

To excavate the differences in-depth in the surface area for the as-prepared samples, the nitrogen adsorption/desorption isotherms and pore size distributions of the samples were examined. As shown in Figure S2a, the total BET surface area of the activated coal gangue is significantly larger than that of the crushed coal gangue, which was due to the formation of loose and porous colloidal structures with a nanometer scale. In addition, the pore sizes of both samples were mainly distributed mainly in the range of 5~20 nm (Figure S2b), which could supply fast diffusion channels for O_2 and sufficient storage space for the discharge product Li_2O_2 . The crystal structure of the crushed and activated coal gangues was characterized by X-ray diffraction (XRD) in Figure 3. Apparently, the strong diffraction peaks at 21.09° and 26.91° corresponded to the crystalline planes of quartz, the peaks at 11.61° and 29.75° related to the crystalline planes of kaolinite, and the peak at 35.15° was attributed to the crystalline planes of hematite, respectively. The natural coal gangue contained a variety of mineral components, leading to low electrochemical activity [28]. However, there were no evident diffraction peaks in the XRD patterns of the activated coal gangue, indicating that the activated coal gangue had an amorphous structure. It should be emphasized that the only strong diffraction peak at 23.70° corresponded to the sample stage.

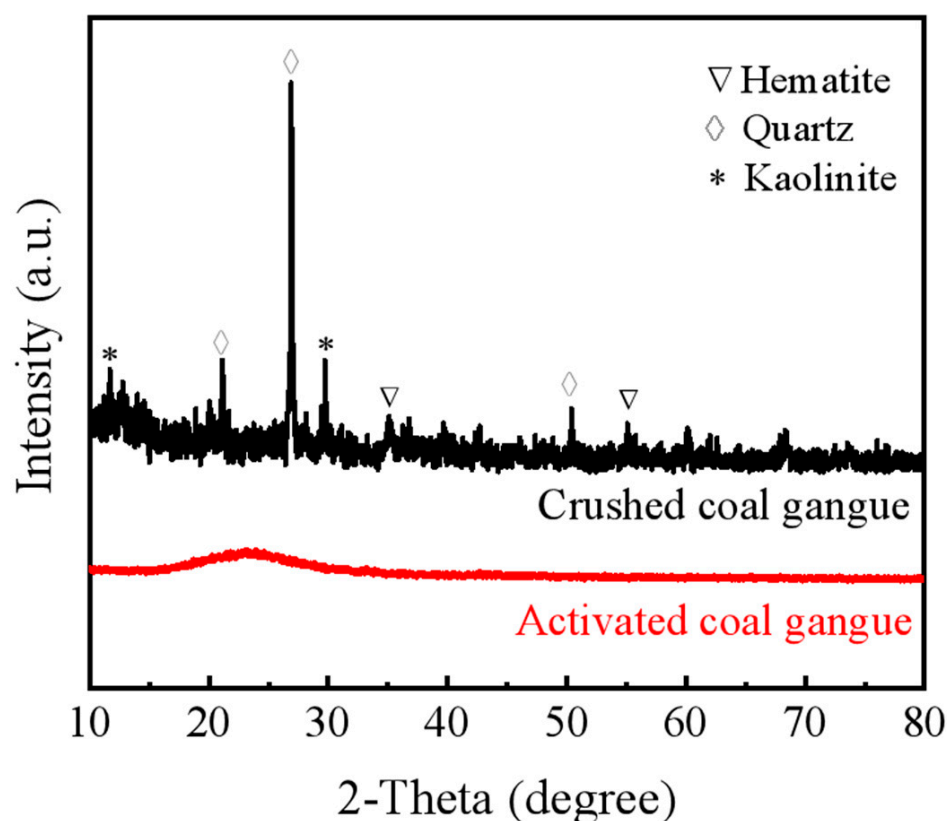


Figure 3. XRD patterns of the as-prepared samples.

X-ray photoelectron spectroscopy (XPS) was performed to further understand the elements' compositions, chemical states, molecular structures, and other aspects of the activated coal gangue. From the full spectra in Figure 4a, there are various peaks corresponding to Si, Al, C, O, and many other impure elements on the surface of the crushed coal gangue. However, the activated coal gangue contains only Si, C, and O peaks. As shown in Table S1, the Si/C and Si/O ratio in the activated coal gangue is higher than those in crushed coal gangue, suggesting the acid–alkali activation treatment could remove the impurities of the gangue and retain the silica-based compounds. In addition, the Si/O atomic ratio is more than 1/2 compared to that of the stoichiometric SiO_2 , which indicates that more oxygen vacancies are exposed on the surface of the coal gangue after the acid–alkali activation treatment. The high-resolution Si 2p spectra are displayed in Figure 4b. Both the spectra of the activated coal gangue and the crushed coal gangue had to be fitted into two peaks located at 104.2 and 103.6 eV, which represent the existence of the strong Si–C and Si–O bonds, respectively [28]. Combined with the previous XRD data, it is shown that the surface of the activated coal gangue in situ forms SiO_x and SiC_x with stable amorphous structures, which has been proven to be helpful in improving the electrocatalytic activity of coal gangue [29]. To make more efforts in verifying the conjecture ahead, the C 1s and O 1s spectra of the samples were tested and analyzed in-depth. As shown in Figure 4c, the C 1s spectra could be deconvoluted into three characteristic peaks centralized at 289.5, 286.3 and 284.8 eV for both the activated coal gangue and crushed coal gangue, which related to the existence of π - π^* , C–O, and C–C, respectively. In contrast, the intensities of π - π^* and C–O are both raised in the activated coal gangue, suggesting that there are abundant carbon-based functional groups and strong chemical bonds between carbon and oxide formed on the activated coal gangue. The O 1s spectra in Figure 4d could be well fitted into two peaks at 530.7 and 533.4 eV, corresponding to the lattice oxygen and defected oxygen [30]. Evidently, the intensity of defected oxygen peak is significantly enhanced over lattice oxygen for activated coal gangue. The result suggested that abundant oxygen vacancies are created

in non-stoichiometric SiO_x , which could further improve the electrochemical activity of coal gangue [31]. As shown in Table S1 (Supporting Information), the Si/C and Si/O ratio in activated coal gangue is higher than those in crushed coal gangue, suggesting the acid-alkali activation treatment could remove the impurities of gangue and retain silica-based compounds. Besides, the Si/O atomic ratio is more than 1/2 by compared by that of stoichiometric SiO_2 , which indicating that more oxygen vacancies is exposed on the surface of coal gangue after acid-alkali activation treatment. On the basis of the SEM, XRD, and XPS analyses, it could be concluded that the amorphous hybrid $\text{SiC}_x/\text{SiO}_x$ with rich oxygen vacancies is successfully formed in situ on the surface of coal gangue after acid-alkali activation treatment.

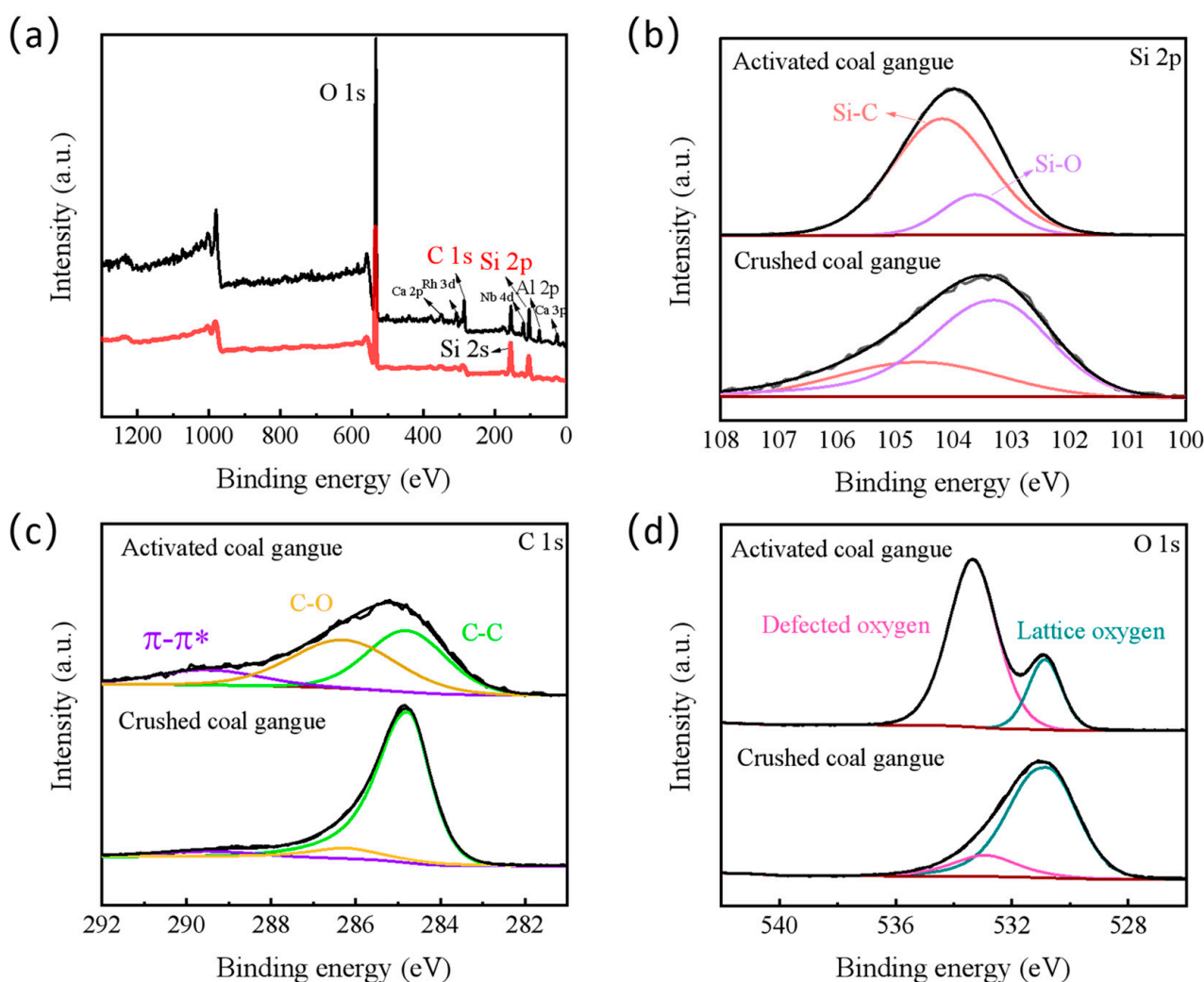


Figure 4. (a) XPS surveys for as-prepared samples; High-resolution Si 2p (b), C 1s (c), O 1s (d) spectra for activated coal gangue and crushed coal gangue.

3.3. The Performance of Activated Coal Gangue in LOBs

The 2032-coin-type LOBs were assembled to examine the actual electrocatalytic performance of the activated coal gangue. As shown in Figure 5a, the battery configuration is composed of a gangue-based cathode, a diaphragm, and a lithium anode. The gangue-based cathode plays a dual role as the electrochemical reaction area and the storage area of the discharge product lithium peroxide (Li_2O_2) in the cycling process of LOBs. The activity of the gangue-based cathode has been the key to the development of LOBs. The full charging–discharging curve in Figure 5b shows that activated coal gangue delivers a superior specific discharge capacity (9156 mAh g^{-1}) and a small discharge overvoltage

(0.17 V) at median discharge capacity. Impressively, the activated coal gangue showed a low charge overvoltage (0.95 V) at median charge capacity, which contributed to preventing the side decomposition of the organic electrolyte, thus improving the durability of LOBs. The existence of the $\text{SiC}_x/\text{SiO}_x$ -activated layer could facilitate the catalytic stability of coal gangue, resulting in large, specific capacities in LOBs. Moreover, the activated coal gangue cathode demonstrated an outstanding rate performance in the long cycling process under different current densities, ranging from 200 to 2000 mA g^{-1} (Figure 5c). Notably, the activated coal gangue kept a discharge–charge voltage gap from ~ 1.51 V (200 mA g^{-1}) to ~ 1.96 V (2000 mA g^{-1}). In addition, the activated coal gangue maintained little numerical difference in the discharge–charge overvoltage (~ 1.54 V) when returning to 200 mA g^{-1} . Amazingly, the activated coal-gangue-based cathode could still circulate stably for more than 300 h at 200 mA g^{-1} , implying that the activated coal-gangue-based LOBs delivered a splendid practical application in fast charging. In terms of the cycling stability of LOBs, the activated coal gangue could be maintained for more than 400 h, without evident degradation, at 200 mA g^{-1} . To sum up, the coal gangue activated by the simple acid–alkali treatment was a promising cathode catalyst for the LOBs. The electrochemical performance of activated coal gangue-based cathode in this work and those of reported typical other catalyst-based cathodes are summarized in Table S2 (Supporting Information). By comparison, the discharge capacity and cycling stability of activated coal gangue-based cathode in this work is the best among the catalysts in LOBs.

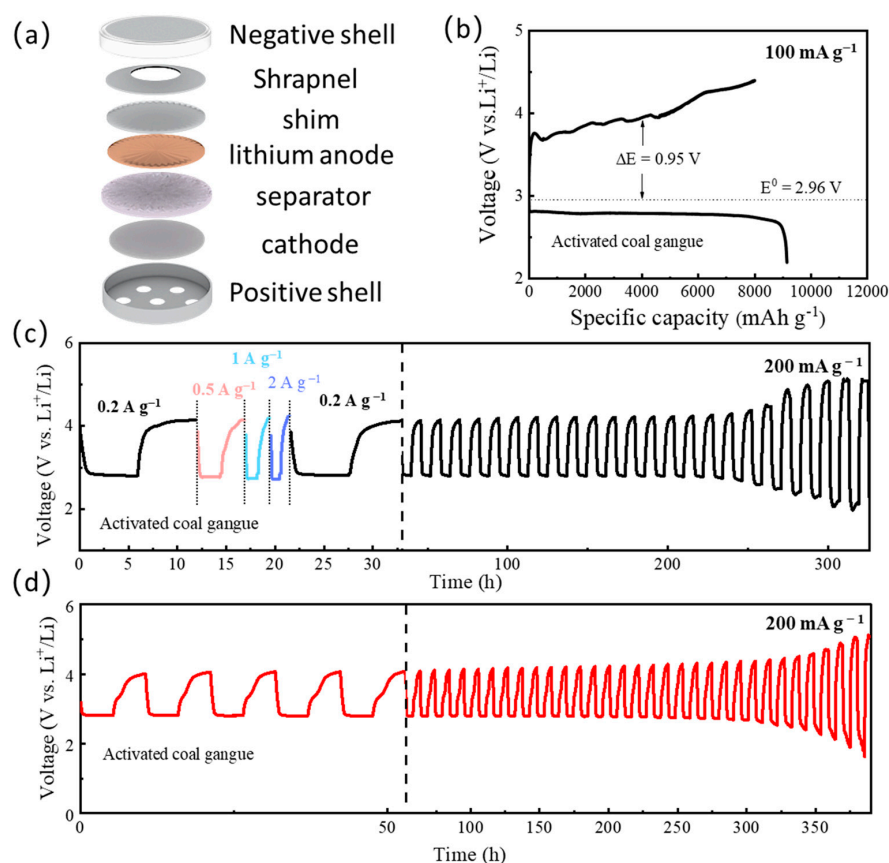


Figure 5. (a) Configuration of 2032-coin LOBs. (b) initial full discharge/charge curves of gangue-based LOBs at 100 mA g^{-1} ; (c) rate performances of gangue-based LOBs; (d) cycling stability of gangue-based LOBs with a cut-off capacity of 1000 mAh g^{-1} .

To totally clarify the intrinsic mechanisms of the activated coal gangue and understand the potential influence of amorphous $\text{SiC}_x/\text{SiO}_x$ on the cycling efficiencies of LOBs, electrochemical impedance spectra (EIS) and XPS were applied (Figure 6). As shown in Figure 6a, the activated coal gangue demonstrated ohmic resistance (R_o , $\sim 20 \Omega$), with an evident

change in all states, but showed distinctly different values in charge transfer resistance (R_{ct}). In detail, the activated coal-gangue-based LOBs showed a bigger discharge R_{ct} (208.40 Ω) than that of the charged (145.70 Ω) and pristine states (126.43 Ω). The equivalent circuit (right in Figure 6a) made it clear that a new interface was formed on the surface of the gangue-based cathode after the 1st discharge, relating to the formation and loading of the discharge products. During the subsequent 1st charging process, the discharge products were completely decomposed, resulting in only one interface resistance in the equivalent circuit. The high-resolution Li 1s spectra in Figure 6b confirmed that the discharge product formed on the surface of the gangue-based cathode was lithium peroxide (Li_2O_2 , 54.6 eV). Fortunately, Li_2O_2 could be completely decomposed after the following charge. From the right in Figure 6b, the XPS analysis indicated that the synergistic interaction between SiC_x and SiO_x on the surface of the activated coal gangue was beneficial to promote the formation/decomposition of Li_2O_2 , improving the cycling stabilization of LOBs.

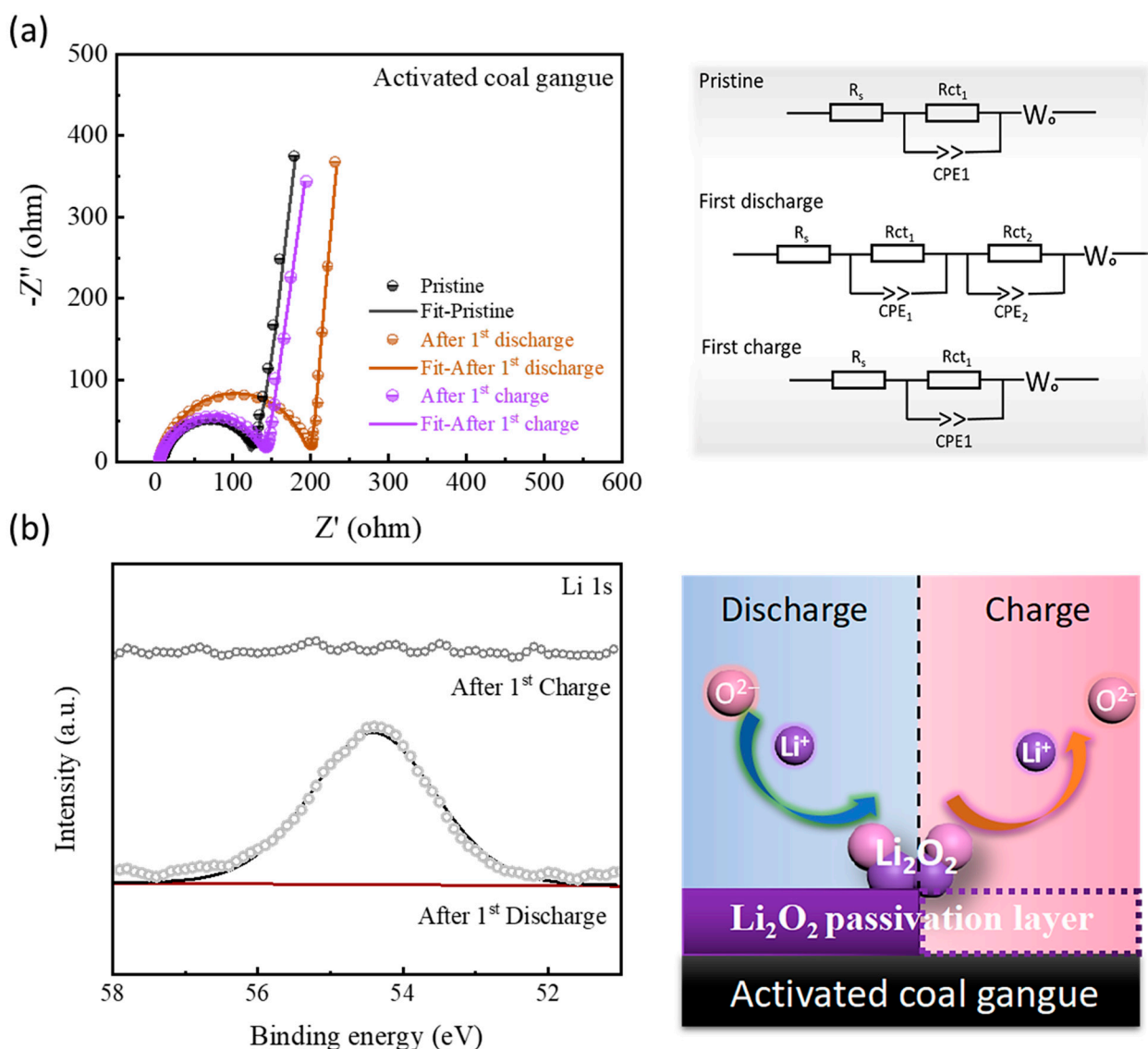


Figure 6. (a) EIS of gangue-based LOBs after assembled and 1st discharge–charge states and the corresponding analog circuit diagram; (b) Li 1s XPS spectra of activated coal gangue after the first discharge/charge cycle.

4. Conclusions

In conclusion, the activated coal gangue with coated amorphous $\text{SiC}_x/\text{SiO}_x$ was firstly synthesized and applied as excellent cathodes for LOBs. The gangue-based cathodes

exhibited superior specific capacities and superior cycling stabilization. The significant electrochemical performances of the gangue-based LOBs were verified by photoelectron spectroscopy:

- (i) The amorphous $\text{SiC}_x/\text{SiO}_x$ layer formed in situ on the surface of the activated gangue is conducive to promoting structural stability, providing an adequate void for product deposition;
- (ii) After acid–alkali activation, abundant functional groups and oxygen vacancies were exposed on the surface of the coal gangue, which could play a key role in improving the formation/decomposition efficiencies of discharge products (Li_2O_2) as highly active electrochemical reaction sites.

This work provided a new application of coal gangue with high electrochemical catalytic performance in energy storage devices.

Supplementary Materials: The following supporting information can be downloaded at: <https://www.mdpi.com/article/10.3390/app13095551/s1>, Figure S1: XRD patterns of the intermediate products; Figure S2: N_2 adsorption-desorption isotherms (a) and pore size distributions (b) of as-prepared samples; Table S1: The atomic content of each element for activated coal gangue and crushed coal gangue from XPS; Table S2: Comparison of battery performance of activated coal gangue-based electrode with other reported electrodes. References [32–36] are cited in the supplementary materials.

Author Contributions: Conceptualization, Z.S. and N.Z.; Methodology, Z.S. and N.Z.; validation, Z.S., M.L. and N.Z.; Formal analysis, Z.S., M.L. and N.Z.; Investigation, Z.S. and N.Z.; resources, N.Z.; Data curation, Z.S., M.L. and N.Z.; Writing—original draft preparation, Z.S., M.L., J.X. and N.Z.; Writing—review and editing, Z.S., W.F., S.L. and N.Z.; Supervision, Z.S., M.L. and N.Z.; Project administration, N.Z.; Funding acquisition, Z.S. and N.Z. All authors have read and agreed to the published version of the manuscript.

Funding: This research was funded by the Fundamental Research Funds for the National Natural Science Foundation of China (52130402), the Fundamental Research Funds for the Central Universities (2022QN1003), and the China Postdoctoral Science Foundation (2021M703495).

Institutional Review Board Statement: Not applicable.

Informed Consent Statement: Not applicable.

Data Availability Statement: Not applicable.

Conflicts of Interest: The authors declare no conflict of interest.

References

1. Zhou, Y.; Yin, K.; Gu, Q.; Tao, L.; Li, Y.; Tan, H.; Zhou, J.; Zhang, W.; Li, H.; Guo, S. Lewis-Acidic PtIr Multipods Enable High-Performance Li–O₂ Batteries. *Angew. Chem. Int. Ed.* **2021**, *60*, 26592–26598. [[CrossRef](#)] [[PubMed](#)]
2. Li, M.; Wang, X.; Li, F.; Zheng, L.; Xu, J.; Yu, J. A Bifunctional Photo-Assisted Li–O₂ Battery Based on a Hierarchical Heterostructured Cathode. *Adv. Mater.* **2020**, *32*, 1907098. [[CrossRef](#)] [[PubMed](#)]
3. Ding, Y.; Li, Y.; Wu, M.; Zhao, H.; Li, Q.; Wu, Z.S. Recent advances and future perspectives of two-dimensional materials for rechargeable Li–O₂ batteries. *Energy Storage Mater.* **2020**, *31*, 470–491. [[CrossRef](#)]
4. Lyu, Z.; Zhou, Y.; Dai, W.; Cui, X.; Lai, M.; Wang, L.; Huo, F.; Huang, W.; Hu, Z.; Chen, W. Recent advances in understanding of the mechanism and control of Li₂O₂ formation in aprotic Li–O₂ batteries. *Chem. Soc. Rev.* **2017**, *46*, 6046–6072. [[CrossRef](#)] [[PubMed](#)]
5. Wang, J.; Ma, L.; Xu, J.; Xu, Y.; Sun, K.; Peng, Z. Oxygen electrochemistry in Li–O₂ batteries probed by in situ surface-enhanced Raman spectroscopy. *SusMat* **2021**, *1*, 345–358. [[CrossRef](#)]
6. Sun, Z.; Cao, X.; Tian, M.; Zeng, K.; Jiang, Y.; Rummeli, M.H.; Strasser, P.; Yang, R. Synergized Multimetal Oxides with Amorphous/Crystalline Heterostructure as Efficient Electrocatalysts for Lithium–Oxygen Batteries. *Adv. Energy Mater.* **2021**, *11*, 2100110. [[CrossRef](#)]
7. Lv, Q.; Zhu, Z.; Zhao, S.; Wang, L.; Zhao, Q.; Li, F.; Archer, L.A.; Chen, J. Semiconducting Metal–Organic Polymer Nanosheets for a Photoinvolved Li–O₂ Battery under Visible Light. *J. Am. Chem. Soc.* **2021**, *143*, 1941–1947. [[CrossRef](#)]
8. Wu, X.; Wang, X.; Li, Z.; Chen, L.; Zhou, S.; Zhang, H.; Qiao, Y.; Yue, H.; Huang, L.; Sun, S.G. Stabilizing Li–O₂ Batteries with Multifunctional Fluorinated Graphene. *Nano Lett.* **2022**, *22*, 4985–4992. [[CrossRef](#)]

9. Wang, D.; Mu, X.; He, P.; Zhou, H. Materials for advanced Li-O₂ batteries: Explorations, challenges and prospects. *Mater. Today* **2019**, *430*, 132977. [[CrossRef](#)]
10. Wang, L.; Zhang, Y.; Liu, Z.; Guo, L.; Peng, Z. Understanding oxygen electrochemistry in aprotic Li-O₂ batteries. *Green Energy Environ.* **2017**, *2*, 186–203. [[CrossRef](#)]
11. Zhu, Z.; Mosallanezhad, A.; Sun, D.; Lei, X.; Liu, X.; Pei, Z.; Wang, G.; Qian, Y. Applications of MoS₂ in Li-O₂ Batteries: Development and Challenges. *Energy Fuels* **2021**, *35*, 5613–5626. [[CrossRef](#)]
12. Bai, T.; Li, D.; Xiao, S.; Ji, F.; Zhang, S.; Wang, C.; Lu, J.; Gao, Q.; Ci, L. Recent progress on single-atom catalysts for lithium-air battery applications. *Energy Environ. Sci.* **2023**, *16*, 1431–1465. [[CrossRef](#)]
13. Li, M.; Li, A.; Zhang, J.; Huang, Y.; Li, J. Effects of particle sizes on compressive deformation and particle breakage of gangue used for coal mine goaf backfill. *Powder Technol.* **2020**, *360*, 493–502. [[CrossRef](#)]
14. Li, J.; Wang, J. Comprehensive utilization and environmental risks of coal gangue: A review. *J. Clean. Prod.* **2019**, *239*, 117946. [[CrossRef](#)]
15. Zhang, Y.; Ling, T.C. Reactivity activation of waste coal gangue and its impact on the properties of cement-based materials—A review. *Constr. Build. Mater.* **2020**, *234*, 117424. [[CrossRef](#)]
16. Sun, Z.; Hu, Y.; Zeng, K.; Li, M.; Zhao, S.; Zhang, J. Turn “Waste” Into Wealth: MoO₂@coal Gangue Electrocatalyst with Amorphous/Crystalline Heterostructure for Efficient Li-O₂ Batteries. *Small* **2023**, 2208145. [[CrossRef](#)] [[PubMed](#)]
17. Wang, X.; Zhang, J.; Li, M.; Gao, F.; Taheri, A.; Huo, B.; Jin, L. Expansion Properties of Cemented Foam Backfill Utilizing Coal Gangue and Fly Ash. *Minerals* **2022**, *12*, 763. [[CrossRef](#)]
18. Aralekallu, S.; Thimmappa, R.; Bhat, Z.M.; Devendrachari, M.C.; Dargily, N.C.; Mukhopadhyay, S.; Kottaichamy, A.R.; Thotiyil, M.O. Wireless Chemical Charging of a Metal-Ion Battery by Magnetic Particles. *ACS Sustain. Chem. Eng.* **2022**, *10*, 259–266. [[CrossRef](#)]
19. Zhou, C.; Liu, G.; Wu, S.; SingLam, P.K. The environmental characteristics of usage of coal gangue in bricking-making: A case study at Huainan, China. *Chemosphere* **2014**, *95*, 274–280. [[CrossRef](#)]
20. Peng, H.; Wang, B.; Yang, F.; Cheng, F. Study on the environmental effects of heavy metals in coal gangue and coal combustion by ReCiPe2016 for life cycle impact assessment. *J. Fuel Chem. Technol.* **2020**, *48*, 1402–1408. [[CrossRef](#)]
21. Zhu, H.; Yang, S.; Li, W.; Li, Z.; Fan, J.; Shen, Z. Study of Mechanical Properties and Durability of Alkali-Activated Coal Gangue-Slag Concrete. *Materials* **2020**, *13*, 5576. [[CrossRef](#)]
22. Hao, Y.; Guo, X.; Yao, X.; Han, R.; Li, L.; Zhang, M. Using Chinese Coal Gangue as an Ecological Aggregate and Its Modification: A Review. *Materials* **2022**, *15*, 4495. [[CrossRef](#)]
23. Zhang, X.; Zhao, R.; Zhang, N.; Su, Y.; Liu, Z.; Gao, R. Insight to unprecedented catalytic activity of double-nitrogen defective metal-free catalyst: Key role of coal gangue. *Appl. Catal. B Environ.* **2020**, *263*, 118316. [[CrossRef](#)]
24. Mei, J.; Zhang, Q.; Peng, H.; Liao, T.; Sun, Z. Phase engineering activation of low-cost iron-containing sulfide minerals for advanced electrocatalysis. *J. Mater. Sci. Technol.* **2022**, *111*, 181–188. [[CrossRef](#)]
25. Dong, X.; Ren, B.; Sun, Z.; Li, C.; Zhang, X.; Kong, M.; Zheng, S.; Dionysiou, D.D. Monodispersed CuFe₂O₄ nanoparticles anchored on natural kaolinite as highly efficient peroxy monosulfate catalyst for bisphenol A degradation. *Appl. Catal. B Environ.* **2019**, *253*, 206–217. [[CrossRef](#)]
26. Zhang, S.; Zhang, N.; Zhao, W.; Lan, D.; Hao, G.; Yi, X.; Yang, Z.; Hu, J.; He, W.; Liu, Y.; et al. Green preparation of hierarchical porous C/SiO_x composites from coal gangue as anodes for Li-ion batteries. *Solid State Ion.* **2021**, *371*, 115772. [[CrossRef](#)]
27. Moghadam, M.J.; Ajalloeian, R.; Hajiannia, A. Preparation and application of alkali-activated materials based on waste glass and coal gangue: A review. *Constr. Build. Mater.* **2019**, *221*, 84–98. [[CrossRef](#)]
28. Zhou, X.; Xie, H.; He, X.; Zhao, Z.; Ma, Q.; Cai, M.; Yin, H. Annihilating the Formation of Silicon Carbide: Molten Salt Electrolysis of Carbon-Silica Composite to Prepare the Carbon-Silicon Hybrid for Lithium-Ion Battery Anode. *Energy Environ. Mater.* **2020**, *3*, 166–176. [[CrossRef](#)]
29. Kim, H.; Kim, T.Y.; Roev, V.; Lee, H.C.; Kwon, H.J.; Lee, H.; Kwon, S.; Im, D. Enhanced Electrochemical Stability of Quasi-Solid-State Electrolyte Containing SiO₂ Nanoparticles for Li-O₂ Battery Applications. *ACS Appl. Mater. Interfaces* **2016**, *8*, 1344–1350. [[CrossRef](#)]
30. Wu, S.; Liu, H.; Huang, Z.; Xu, H.; Shen, W. O-vacancy-rich porous MnO₂ nanosheets as highly efficient catalysts for propane catalytic oxidation. *Appl. Catal. B Environ.* **2022**, *312*, 121387. [[CrossRef](#)]
31. Li, J.; Shu, C.; Liu, C.; Chen, X.; Hu, A.; Long, J. Rationalizing the Effect of Oxygen Vacancy on Oxygen Electrocatalysis in Li-O₂ Battery. *Small* **2020**, *16*, 2001812. [[CrossRef](#)]
32. Li, Z.; Yang, J.; Agyeman, D.A.; Park, M.; Tamakloe, W.; Yamauchi, Y.; Kang, Y.M. CNT@Ni@Ni-Co silicate core-shell nanocomposite: A synergistic triple-coaxial catalyst for enhancing catalytic activity and controlling side products for Li-O₂ batteries. *J. Mater. Chem. A* **2018**, *6*, 10447–10455. [[CrossRef](#)]
33. Zheng, R.; Shu, C.; Hou, Z.; Hu, A.; Hei, P.; Yang, T.; Li, J.; Liang, R.; Long, J. In Situ Fabricating Oxygen Vacancy-Rich TiO₂ Nanoparticles via Utilizing Thermodynamically Metastable Ti Atoms on Ti₃C₂T_x MXene Nanosheet Surface To Boost Electrocatalytic Activity for High-Performance Li-O₂ Batteries. *ACS Appl. Mater. Interfaces* **2019**, *11*, 46696–46704. [[CrossRef](#)] [[PubMed](#)]
34. Lu, Y.; Ang, H.; Yan, Q.; Fong, E. Bioinspired Synthesis of Hierarchically Porous MoO₂/Mo₂C Nanocrystal Decorated N-Doped Carbon Foam for Lithium-Oxygen Batteries. *Chem. Mater.* **2016**, *28*, 5743–5752. [[CrossRef](#)]

35. Liu, J.; Li, D.; Wang, Y.; Zhang, S.; Kang, Z.; Xie, H.; Sun, L. MoO₂ nanoparticles/carbon textiles cathode for high performance flexible Li-O₂ battery. *J. Energy Chem.* **2020**, *47*, 66–71. [[CrossRef](#)]
36. Cao, X.; Sun, Z.; Zheng, X.; Jin, C.; Tian, J.; Li, X.; Yang, R. MnCo₂O₄/MoO₂ Nanosheets Grown on Ni foam as Carbon- and Binder-Free Cathode for Lithium–Oxygen Batteries. *ChemSusChem* **2018**, *11*, 574–579. [[CrossRef](#)] [[PubMed](#)]

Disclaimer/Publisher’s Note: The statements, opinions and data contained in all publications are solely those of the individual author(s) and contributor(s) and not of MDPI and/or the editor(s). MDPI and/or the editor(s) disclaim responsibility for any injury to people or property resulting from any ideas, methods, instructions or products referred to in the content.